**GSA Data Repository 2015030**

**Fujioka et al. "Flood flipped boulders: *in situ* cosmogenic nuclide modeling of flood deposits in the monsoon tropics of Australia"**

## 1. Analytical methods

Rock samples (Table DR1) were crushed, sieved, and the 212–500 μm grain size fraction was subjected to sequential acid treatment by aqua regia, hot phosphoric acid (Mifsud et al., 2013) and dilute (2–5% w/w) HF to obtain pure quartz powder. After addition of Be carrier (~400 μg) prepared from beryl crystal, approximately 40 g of pure quartz was dissolved in concentrated HF. Be and Al fractions were isolated by sequential pH control and ion chromatography (Child et. al., 2000). The eluted solutions were converted to hydroxide, and calcined to BeO and $Al_2O_3$ at 800°C. The oxides were mixed with Nb in mass ratios of BeO:Nb = 1:4 and $Al_2O_3$:Nb = 1:3 and pressed into Al and Cu cathodes, respectively (Fink et al., 2000). The $^{10}Be/^{9}Be$ and $^{26}Al/^{27}Al$ ratios were measured at the ANSTO ANTARES AMS facility (Fink and Smith, 2007). Measured $^{10}Be/^{9}Be$ ratios were normalized against Standard Reference Material NIST-4325 with a nominal ratio of 27,900 x $10^{-15}$ (Nishiizumi et al., 2007) and $^{26}Al/^{27}Al$ ratios against Standard Reference Material PRIME Z93-0221 with a nominal ratio of 16,450 x $10^{-15}$ (Fink and Smith, 2007). Procedural blanks using only the beryl spike yielded $^{10}Be/^{9}Be$ ratios of 4–5 x $10^{-15}$ and were ≤3% of the sample $^{10}Be/^{9}Be$ ratios in this study. Al procedural blanks, using a commercial 1000 ppm Al ICP standard solution, yielded $^{26}Al/^{27}Al$ ratios of 4–8 x $10^{-15}$ which resulted in count rates of 1–3 x $10^{-3}$ $^{26}Al$ counts sec$^{-1}$, and were 1–8% of the sample $^{26}Al$ counts sec$^{-1}$. No aluminum spike was added during sample processing. Analytical errors include AMS counting statistics, standard normalization and blank corrections. Reproducibility uncertainties of 2% for $^{10}Be$ and 3% for $^{26}Al$ based on repeated measurements of AMS standards (Fink and Smith, 2007), 1% for our Be spike concentration, and a 4% mean uncertainty for intrinsic Al analysis by ICP-OES were propagated in quadrature with the AMS analytical errors to estimate errors for the final $^{10}Be$ and $^{26}Al$ concentrations (Table 1).

## 2. Erosion rate calculations for bedrock sample JW-4-BR

Cosmogenic nuclide concentrations, $N$ (atoms g$^{-1}$), in an eroding surface with constant erosion rate, $\varepsilon$ (cm yr$^{-1}$), exposed for $t$ years, is described by (Lal, 1991, Granger and Smith, 2000):

$$N=\sum_{i=0}^{3}\left[\frac{s_i^{sh}s_iP_i}{\lambda+\frac{\rho\varepsilon}{\Lambda_i}}\cdot\left(1-e^{-\left(\lambda+\frac{\rho\varepsilon}{\Lambda_i}\right)t}\right)\right] \tag{S1}$$

where $\lambda$ is the decay constant, 5.00 x $10^{-7}$ $yr^{-1}$ for $^{10}Be$ and 9.83 x $10^{-7}$ $yr^{-1}$ for $^{26}Al$, calculated as $\ln(2)/t_{1/2}$, where $t_{1/2}$ is the half-life (1.387 ± 0.012 Ma for $^{10}Be$ and 0.705 ± 0.024 Ma for $^{26}Al$; Chmeleff et al., 2010; Korschinek et al., 2010; Norris et al., 1983). $s^{sh}{}_i$ is the cumulative shielding correction factor, arising from sample thickness, boulder surface slope angle and depth (i.e., boulder thickness) calculated using eq.(18) of Dunne et al. (1999) (Table DR1). $s_i$ is the geographic scaling factor calculated based on the Stone's model, i.e., $s_0$ = $S_\lambda$ for spallation and $s_1$ = $s_2$ = $s_3$ = $M_\lambda$ for muons (Stone, 2000). $P_i$ are sea-level high latitude production rates. For $^{10}Be$, $P_0$ = 4.48 atoms $g^{-1}$ $yr^{-1}$ for spallation ('St' value of 4.96 in Table 6 of Balco et al., 2008, divided by 1.106, a correction factor resulting from the revision of the nominal value for the NIST-4325 standard; Nishiizumi et al., 2007) and $P_1$ = 0.096, $P_2$ = 0.021 and $P_3$ = 0.026 atoms $g^{-1}$ $yr^{-1}$ for muons (Granger and Smith, 2000). For $^{26}Al$, $P_0$ = 30.2 atoms $g^{-1}$ $yr^{-1}$ for spallation (calculated from $P_0$ ($^{10}Be$) above, assuming an $^{26}Al/^{10}Be$ production rate ratio of 6.75; Balco et al., 2008) and $P_1$ = 0.723, $P_2$ = 0.156 and $P_3$ = 0.192 atoms $g^{-1}$ $yr^{-1}$ for muons (Granger and Smith, 2000). $\Lambda_i$ are attenuation lengths of secondary cosmic ray particles where $\Lambda_0$ (spallation) = 160 g $cm^{-2}$ and muon attenuations lengths are $\Lambda_1$ = 738.6, $\Lambda_2$ = 2688 and $\Lambda_3$ = 4360 g $cm^{-2}$ (Granger and Smith, 2000). $\rho$ is rock density (2.7 g $cm^{-3}$).

Steady state erosion rates for bedrock sample JW-4-BR were calculated by assuming $t \gg (\lambda + \rho\varepsilon/\Lambda)^{-1}$ in eq.(S1) as follows;

$$N=\sum_{i=0}^{3}\left[\frac{s_i^{sh}s_iP_i}{\lambda+\frac{\rho\varepsilon}{\Lambda_i}}\right] \tag{S2}$$

Equation (S2) can be solved numerically for $\varepsilon$. Errors for the steady state erosion rates were derived from quadrature addition of uncertainties in the analytical AMS measurements (3–4% for $^{10}Be$ and 6–11% for $^{26}Al$), uncertainties in half-lives (0.87% for $^{10}Be$ and 3.4% for $^{26}Al$), and estimated errors in production rates (9%; Balco et al 2008) (Table 1).

## 3. Evaluating boulder flipping

To evaluate whether a sampled boulder has been flipped or not, we first predict the cosmogenic $^{10}$Be concentration for the bottom surface of the boulder, $N_{bottom,\ predicted}$, based on the measured $^{10}$Be for its top or upper surface, $N_{top}$, accounting for boulder thickness. Thus

$$N_{bottom,predicted} = \frac{s_0^{sh,bottom}}{s_0^{sh,top}} \cdot N_{top} = e^{-\frac{\rho h^*}{\Lambda_0}\cdot\left(1+\frac{\alpha^2}{5000}\right)} \cdot N_{top} \tag{S3}$$

$s_0^{sh,bottom}$ and $s_0^{sh,top}$ represent shielding corrections for the bottom and top surface samples, respectively, and $\alpha$ denotes a slope angle of the boulder surface to the horizontal (Table DR1; cf. eq.(18) of Dunne et al., 1999). $h^*$ is a depth difference (cm) between the mid points of top and bottom samples, and is calculated as $h^* = h - (x_b + x_t)/2$ where $h$, $x_b$ and $x_t$ denote boulder thickness (cm), sample thickness (cm) for the bottom and top surface samples, respectively (Table DR1). Note that here we only consider spallation reaction in eq.(S3) as the thickness of our boulders are less than one meter, and muon contributions at these shallow depths are minor. If the boulder is extracted during the flood event from a deeply buried position, of the order of several meters in depth, production via muon reactions would have been the major source of the inherited cosmogenic inventory at the beginning of the post-flip exposure. And Equation S3 would require additional muon terms. However, we consider that such deep exhumation is a) not realistic in our field settings and b) the magnitude of our modelled inheritance concentrations cannot be achieved by muon production alone.

We then calculate the ratio, $R_{Meas/Pred}$, defined by $N_{bottom,measured}$ / $N_{bottom,predicted}$, (see column 6 in Table 1). When $R_{Meas/Pred}$ is indistinguishable from unity, the $^{10}$Be profile within the boulder is at steady state, and one cannot unequivocally confirm whether the boulder had ever been flipped or it had flipped sufficiently long ago so that the modified depth profile had returned to a steady state (cf. Fig. 2C). However, a value of $R_{Meas/Pred}$ greater than unity can only be achieved if the boulder had overturned.

Using the criteria described above, four out of the six sampled boulders are identified to have been overturned (i.e., JW-1, -2, -5 and -7), whereas two (JW-3 and -6) show $R_{Meas/Pred}$ ~ 1 within their uncertainties and thus it is not possible to verify if they have been flipped (Table 1).

## 4. Boulder flipping model

### 4.1. Model description

Measured $^{10}$Be concentrations in the top and bottom surfaces of a flipped boulder consist of two components: prior to flip event (termed as inheritance) and post-flip build-up. Immediately after the boulder has overturned (i.e., at $T = 0$), its $^{10}$Be concentration in both the hidden (previously exposed) surface, $N_{bottom,inh}$ (atoms g$^{-1}$) and in its newly exposed (previously hidden) surface, $N_{top,inh}$ (atoms g$^{-1}$), are only due to inheritance, and $N_{top,inh}$ can thus be predicted to be:

$$N_{top,inh} = N_{bottom,inh} \cdot e^{-\frac{\rho h^*}{\Lambda_0}} \quad \text{(S4)}$$

After a time $T$ years, the final $^{10}$Be concentration in the two surfaces of a flipped boulder can be expressed directly as the sum of inheritance (corrected for decay since flipping), and production at the surface (for exposed surface) or at depth $h^*$ (for hidden surface) as:

$$N_{top}(T) = N_{bottom,inh} \cdot e^{-\left(\frac{\rho h^*}{\Lambda}+\lambda T\right)} + \sum_{i=0}^{3}\left[\frac{s_i^{sh,top} s_i P_i}{\lambda + \frac{\rho\varepsilon}{\Lambda_i}} \cdot \left(1 - e^{-\left(\lambda+\frac{\rho\varepsilon}{\Lambda_i}\right)T}\right)\right] \quad \text{(S5)}$$

$$N_{bottom}(T) = N_{bottom,inh} \cdot e^{-\lambda T} + \sum_{i=0}^{3}\left[\frac{s_i^{sh,bottom} s_i P_i}{\lambda + \frac{\rho\varepsilon}{\Lambda_i}} \cdot \left(1 - e^{-\left(\lambda+\frac{\rho\varepsilon}{\Lambda_i}\right)T}\right)\right] \quad \text{(S6)}$$

where the 1st and 2nd terms of eqs.(S5,S6) represent inheritance corrected for decay and post flipping nuclide productions, respectively. Having measured $^{10}$Be concentrations of the top ($N_{top}$) and bottom ($N_{bottom}$) surfaces of flipped boulders and boulder thickness ($h$), there remain three unknowns, i.e., $N_{bottom,inh}$, $\varepsilon$ and $T$. In the following sections, we show model calculations of flipping ages in three progressively more sophisticated models: model A assumes spallation production only with no erosion ($\varepsilon = 0$); model B includes both spallation and muon production with $\varepsilon = 0$; and model C incorporates erosion rates together with spallation and muon productions, to see sensitivity of the model against muon contributions and erosion rate variations.

*(i) Model A: spallation only with no erosion ($P_1 = P_2 = P_3 = \varepsilon = 0$)*

In this most simplified model, eqs.(S5,S6) are reduced respectively to:

$$N_{top} = N_{bottom,inh} \cdot e^{-\left(\frac{\rho h^*}{\Lambda}+\lambda T\right)} + \frac{s_0^{sh,top} s_0 P_0}{\lambda} \cdot \left(1-e^{-\lambda T}\right) \tag{S7}$$

$$N_{bottom} = N_{bottom,inh} \cdot e^{-\lambda T} + \frac{s_0^{sh,bottom} s_0 P_0}{\lambda} \cdot \left(1-e^{-\lambda T}\right) \tag{S8}$$

Equations (S7,S8) can be analytically solved for $T$ by eliminating $N_{bottom,inh}$ as:

$$T = -\frac{1}{\lambda} \cdot \ln\left[1 - \frac{\lambda N_{top}}{s_0 P_0} \cdot \frac{1 - R \cdot e^{-\frac{\rho h^*}{\Lambda_0}}}{s_0^{sh,top} - s_0^{sh,bottom} \cdot e^{-\frac{\rho h^*}{\Lambda_0}}}\right] \tag{S9}$$

where $R$ is the ratio of the measured nuclide concentrations between bottom and top surfaces (i.e., $R = N_{bottom}/N_{top}$). Note that for the extreme case where boulder thickness $h$ is sufficiently large (i.e., >3 m, which is ~5 e-folding depths for spallation assuming a rock density 2.7 g cm$^{-3}$), eq.(S9) is further reduced to:

$$T = -\frac{1}{\lambda} \cdot \ln\left[1 - \frac{\lambda N_{top}}{s_0^{sh,top} s_0 P_0}\right] \tag{S10}$$

As expected, in this case, model flip ages $T$ would be equal to apparent exposure ages calculated solely from the nuclide concentration in the top surface sample.

*(ii) Model B: spallation and muons with no erosion (ε = 0)*

In this semi-simplified model, eqs.(S5,S6) are reduced respectively to:

$$N_{top} = N_{bottom,inh} \cdot e^{-\left(\frac{\rho h^*}{\Lambda}+\lambda T\right)} + \frac{1-e^{-\lambda T}}{\lambda} \cdot \sum_{i=0}^{3}\left[s_i^{sh,top} s_i P_i\right] \tag{S11}$$

$$N_{bottom} = N_{bottom,inh} \cdot e^{-\lambda T} + \frac{1-e^{-\lambda T}}{\lambda} \cdot \sum_{i=0}^{3}\left[s_i^{sh,bottom} s_i P_i\right] \tag{S12}$$

Equations (S11,S12) can also be analytically solved for *T* as:

$$T = -\frac{1}{\lambda} \cdot \ln \left[ 1 - \lambda N_{top} \cdot \frac{1 - R \cdot e^{-\frac{\rho h^*}{\Lambda_0}}}{\sum_{i=0}^{3} \left[ s_i^{sh,top} s_i P_i \right] - e^{-\frac{\rho h^*}{\Lambda_0}} \cdot \sum_{i=0}^{3} \left[ s_i^{sh,bottom} s_i P_i \right]} \right] \tag{S13}$$

Again, for a sufficiently thick boulder, eq.(S13) is further reduced to:

$$T = -\frac{1}{\lambda} \cdot \ln \left[ 1 - \frac{\lambda N_{top}}{\sum_{i=0}^{3} \left[ s_i^{sh,top} s_i P_i \right]} \right] \tag{S14}$$

*(iii) Model C: neutrons and muons with erosion (full expression)*

In this case, eqs.(S5,S6) cannot be solved analytically for *T*. The two equations are combined by eliminating $N_{bottom,inh}$, and *T* can be solved numerically by optimizing the LHS of the following equation to zero:

$$N_{top} - a_0 N_{bottom} - \sum_{i=0}^{3} \left[ A_i \cdot \left( s_i^{sh,top} - a_o s_i^{sh,bottom} \right) \right] = 0 \tag{S15}$$

where

$$a_0 = e^{-\frac{\rho h^*}{\Lambda_0}} \tag{S16}$$

$$A_i = \frac{s_i P_i}{\lambda + \frac{\rho \varepsilon}{\Lambda_i}} \cdot \left( 1 - e^{-\left( \lambda + \frac{\rho \varepsilon}{\Lambda_i} \right) T} \right) \tag{S17}$$

**4.2. Model calculation**

We calculated model flip ages for the four boulders (JW-1, -2, -5 and -7) identified to have been overturned (Table 1) using eqs.(S9,S13,S15) above for models A, B and C, respectively. Boulder thickness $h$ is listed in Table DR1 and $h^*$ is calculated taking sample thicknesses into account (cf. Section 3 above). For model C, a steady state erosion rate of 2.34 ± 0.25 (11%, 1σ) mm $ka^{-1}$, an average steady state erosion rate calculated from $^{10}Be$ and $^{26}Al$ measurements for the bedrock sample JW-4-BR was assigned (Table 1). Errors for the model flip ages are calculated via incorporating AMS analytical errors for both exposed and hidden surface samples of a boulder, and errors for half-life (0.87% for $^{10}Be$ or 3.4% for $^{26}Al$), production rate (9%; Balco et al., 2008), boulder thickness (10%) and steady-state erosion rates, in quadrature. Model results are shown in Table 1 (see text for discussion of model results).

*Platform samples*

Our model also provides the predicted inheritance concentration for the currently hidden (previously exposed) surface of a boulder i.e., $N_{bottom,inh}$. This can be compared to the nuclide concentration of the platform samples (JW-1-P and 2-P; Figs. DR2F,G). Inheritance for the JW-1 and JW-2 boulders are calculated to be 0.213 x $10^6$ and 0.048 x $10^6$ atoms $g^{-1}$, respectively (Table DR2). Corrected for decay and additional production since flipping, i.e., at 10.3 ka for JW-1 and 146 ka for JW-2 (Table 1), $^{10}Be$ concentrations for the platform samples (JW-1-P and JW-2-P) are predicted to be 0.246 x $10^6$ atoms $g^{-1}$ and 0.417 x $10^6$ atoms $g^{-1}$, respectively (Table DR2). These values are in good agreement with the measured $^{10}Be$ of 0.230 ± 0.007 x $10^6$ atoms $g^{-1}$ for JW-1-P, but about twice as high as that for JW-2-P (0.241 ± 0.008 x $10^6$ atoms $g^{-1}$; Table DR2). The $^{26}Al$ data show results consistent with $^{10}Be$ (Table DR2). While sample JW-1-P was confidently identified as equivalent to JW-1 boulder's originally exposed (now hidden) surface prior to flipping (Fig. DR2F), JW-2 boulder was a member of an imbricated cluster of several boulders (Fig. DR2G), and we could not clearly locate the original position of the latter boulder in the field. Consequently, sample JW-2-P was taken from a bedrock surface what appeared to be in a similar geometric context with respect to JW-2 boulder as for the case of JW-1-P (Fig. DR2G). Therefore, the discrepancy between the model predicted and measured nuclide concentrations for JW-2-P may simply be a result that the JW-2-P bedrock surface is not equivalent to the currently hidden face of the JW-2 boulder.

**References**

Balco, G., Stone, J.O., Lifton, N.A., and Dunai, T.J., 2008, A complete and easily accessible means of calculating surface exposure ages or erosion rates from $^{10}Be$ and $^{26}Al$ measurements: Quaternary Geochronology, v. 3, p. 174-195.

Child, D., Elliot, G., Mifsud, C., Smith, A.M., and Fink, D., 2000, Sample processing for earth science studies at ANTARES: Nuclear Instruments and Methods in Physics Research B: Beam interactions with materials and atoms, v. 172, p. 856-860.

Chmeleff, J., von Blanckenburg, F., Kossert, K., and Jakob, D., 2010, Determination of the $^{10}$Be half-life by multicollector ICP-MS and liquid scintillation counting: Nuclear Instruments and Methods in Physics Research B, v. 268, p. 192-199.

Dunne, J., Elmore, D., and Muzikar, P., 1999, Scaling factors for the rates of production of cosmogenic nuclides for geometric shielding and attenuation at depth on sloped surfaces: Geomorphology, v. 27, p. 3-11.

Fink, D., McKelvey, B., Hannan, D., and Newsome, D., 2000, Cold rocks, hot sands: In-situ cosmogenic applications in Australia at ANTARES: Nuclear Instruments and Methods in Physics Research B, v. 172, p. 838-846.

Fink, D., and Smith, A.M., 2007, An inter-comparison of $^{10}$Be and $^{26}$Al AMS reference standards and the $^{10}$Be half-life: Nuclear Instruments and Methods in Physics Research B, v. 259, p. 600-609.

Granger, D.E., and Smith, A.L., 2000, Dating buried sediments using radioactive decay and muogenic production of $^{26}$Al and $^{10}$Be: Nuclear Instruments and Methods in Physics Research B, v. 172, p. 822-826.

Korschinek, G., Bergmaier, A., Faestermann, T., Gerstmann, U.C., Knie, K., Rugel, G., Wallner, A., Dillmann, I., Dollinger, G., Lierse von Gostomski, C., Kossert, K., Maiti, M., Poutivtsev, M., and Remmert, A., 2010, A new value for the half-life of $^{10}$Be by Heavy-Ion Elastic Recoil Detection and liquid scintillation counting: Nuclear Instruments and Methods in Physics Research B, v. 268, p. 187-191.

Lal, D., 1991, Cosmic ray labeling of erosion surfaces: in situ nuclide production rates and erosion models: Earth and Planetary Science Letters, v. 104, p. 424-439.

Mifsud, C., Fujioka, T., and Fink, D., 2013, Extraction and purification of quartz in rock using hot-phosphoric acid for in situ cosmogenic exposure dating: Nuclear Instruments and Methods in Physics Research B, v. 294, p. 203-207.

Nishiizumi, K., Imamura, M., Caffee, M., Southon, J.R., Finkel, R.C., and McAninch, J., 2007, Absolute calibration of $^{10}$Be AMS standards: Nuclear Instruments and Methods in Physics Research B, v. 258, p. 403-413.

Norris, T.L., Gancarz, A.J., Rokop, D.J., and Thomas, K.W., 1983, Half-life of $^{26}$Al: Journal of Geophysical Research, v. 88 supplement, p. B331-B333.

Stone, J.O., 2000, Air pressure and cosmogenic isotope production: Journal of Geophysical Research, v. 105, p. 23753-23759.

Wende, R., 1999, Boulder bedforms in jointed-bedrock channels, in Miller, A.J., and Gupta, A., eds., Varieties of Fluvial Form, John Wiley and Sons Ltd, p. 189-216.

**Table DR1. Sample information**

| ID [a] | Lat. | Long. | Alt. | Boulder dimensions | | | | | | Sample thickness (x) | Shielding depth [c] (z) | Shielding correction [d] | |
|---|---|---|---|---|---|---|---|---|---|---|---|---|---|
| | | | | Shape | Planar area | Vertical thickness (d) | Slope angle (α) | Boulder thickness [b] (h) | Estimated mass | | | | |
| | (°S) | (°E) | (masl) | | ($m^2$) | (cm) | (deg.) | (cm) | (tons) | (cm) | (cm) | spall. | muons |
| **Boulder samples** | | | | | | | | | | | | | |
| JW-1-T | 15.8293 | 127.4135 | 222 | Triangular | 5.5 x 4.5 | 52 | 15 | 50 | 17 | 3.0 | 1.5 | 0.969 | 0.997 |
| JW-1-B | | | | | | | | | | 2.0 | 49.2 | 0.418 | 0.915 |
| JW-2-T | 15.8291 | 127.4126 | 225 | Rectangular | 3.5 x 3.5 | 82 | 28 | 72 | 24 | 2.0 | 1.0 | 0.957 | 0.998 |
| JW-2-B | | | | | | | | | | 4.0 | 70.4 | 0.247 | 0.881 |
| JW-3-T | 15.8270 | 127.4146 | 223 | Rectangular | 3.5 x 2.9 | 55 | 20 | 52 | 14 | 1.5 | 0.8 | 0.977 | 0.999 |
| JW-3-B | | | | | | | | | | 2.0 | 50.7 | 0.393 | 0.913 |
| JW-5-T | 15.8291 | 127.4127 | 225 | Rectangular | 5.9 x 3.0 | 97 | 21 | 91 | 43 | 2.0 | 1.0 | 0.971 | 0.998 |
| JW-5-B | | | | | | | | | | 2.0 | 89.6 | 0.191 | 0.851 |
| JW-6-T | 15.8259 | 127.4142 | 220 | Rectangular | 4.1 x 2.3 | 45 | 17 | 43 | 11 | 2.0 | 1.0 | 0.976 | 0.998 |
| JW-6-B | | | | | | | | | | 3.0 | 41.5 | 0.473 | 0.928 |
| JW-7-T | 15.8283 | 127.4146 | 224 | Rectangular | 3.0 x 4.0 | 72 | 22 | 67 | 22 | 2.0 | 1.0 | 0.969 | 0.998 |
| JW-7-B | | | | | | | | | | 2.0 | 65.8 | 0.292 | 0.888 |
| **Bedrock samples** | | | | | | | | | | | | | |
| JW-4-BR | 15.8267 | 127.4147 | 227 | - | - | - | - | - | - | 3.5 | 1.8 | 0.971 | 0.997 |
| **Platform samples** | | | | | | | | | | | | | |
| JW-1-P | 15.8293 | 127.4135 | 222 | - | - | - | - | - | - | 2.5 | 1.3 | 0.979 | 0.998 |
| JW-2-P | 15.8291 | 127.4126 | 225 | - | - | - | - | - | - | 2.0 | 1.0 | 0.983 | 0.998 |

a) '-T' and '-B' represent the top and bottom surfaces of a boulder, respectively.

b) Calculated as h = d • cosα, where α is the slope angle of boulder upper surface to the horizontal.

c) Depth (perpendicular to slope) to the mid point of the sample.

d) Calculated using eq.(18) of Dunne et al. (1999) with z, α, and Λ = 160 g $cm^{-2}$ for spallation and 1500 g $cm^{-2}$ for muons.

**Table DR2. AMS results for the platform samples**

| ID | Nuclide | Measured nuclide concentration ($10^6$ at $g^{-1}$) | Inheritance (by model C) ($10^6$ at $g^{-1}$) | Post-flip production ($10^6$ at $g^{-1}$) | Predicted nuclide concentration [a] ($10^6$ at $g^{-1}$) |
|---|---|---|---|---|---|
| JW-1-P | $^{10}Be$ | 0.230 ± 0.007 | 0.213 | 0.034 | 0.246 |
| | $^{26}Al$ | 1.474 ± 0.127 | 1.056 | 0.395 | 1.432 |
| JW-2-P | $^{10}Be$ | 0.241 ± 0.008 | 0.048 | 0.372 | 0.417 |
| | $^{26}Al$ | 1.313 ± 0.100 | 0.082 | 2.319 | 2.391 |

a) Sum of modeled inheritance (column 4) of bottom surface ($N_{bottom,inh}$), corrected for decay for a flip age of $T$ = 10.3 ka for JW-1 and 146 ka for JW-2 (Table 1), and concentration buildup since flip event ($T$ years ago) at surface production rate.

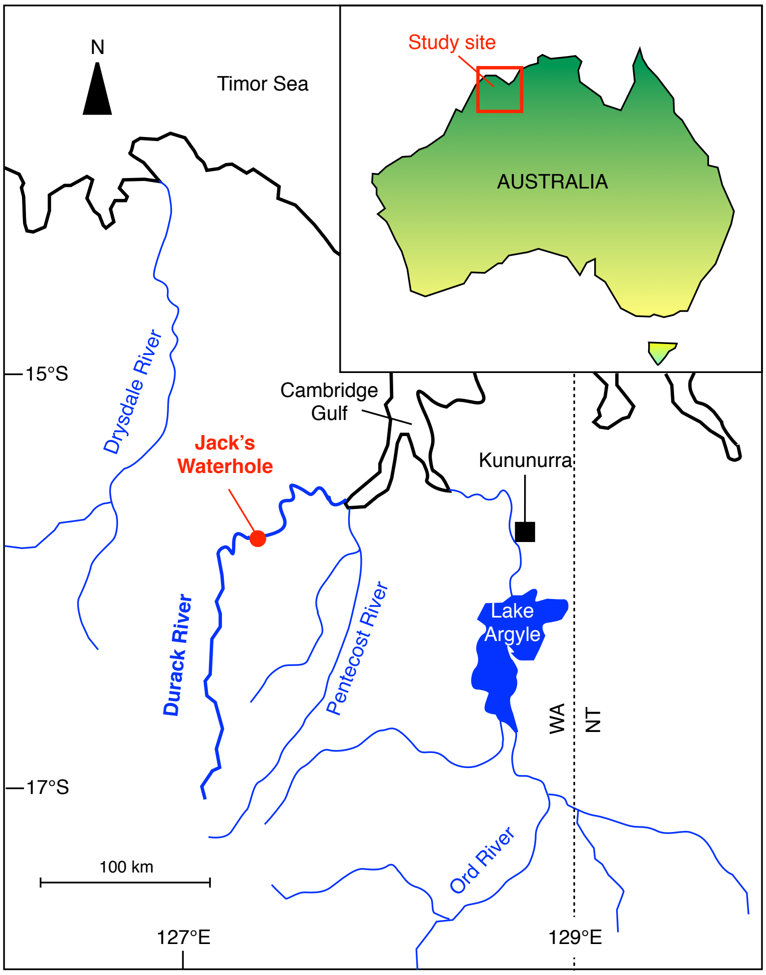


**Figure DR1.** Location of the flood generated boulder field at Jack's Waterhole in the Durack River, the Kimberley, in northern Australia (after Wende, 1999).

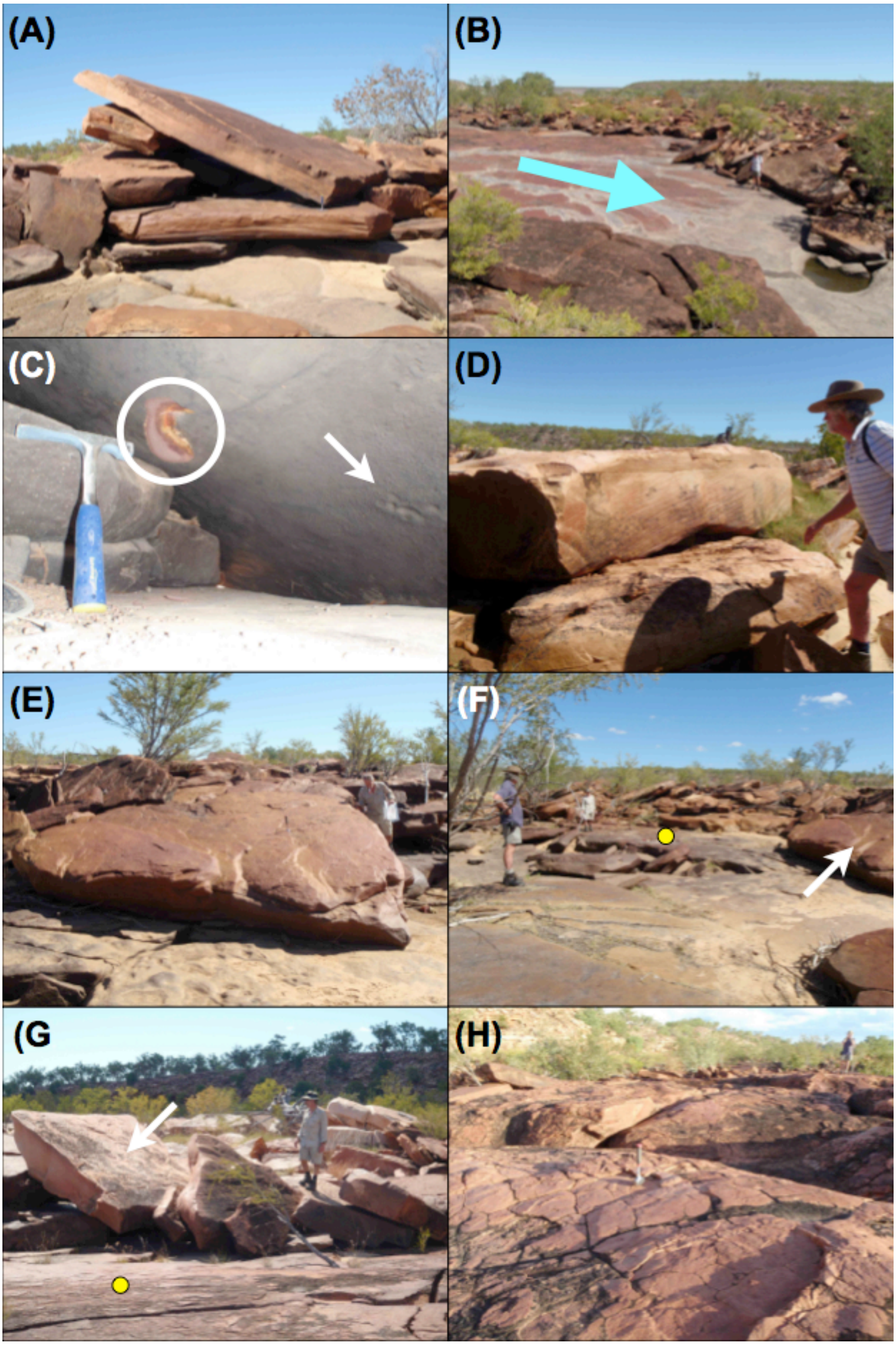
(A)
(B)
(C)
(D)
(E)
(F)
(G)
(H)

**Figure DR2.** Field photos of the boulders at Jack's Waterhole. (A) A stack of imbricated boulders. Geologic hammer for scale at lower right. (B) An example of a boulder free bedrock section near the eastern flank of the gorge, bordered by successions of arced imbricated boulder stacks. The arrow indicates flow direction. A person for scale. (C) The bottom (hidden) face of JW-3 boulder, showing dissolution pits (arrow) and sampling spot (circle). (D) Bedding planes exposed on the joint face of a boulder. (E) Flipped boulder JW-1 on bedrock. Apex of the void locating the original boulder position can be seen at the lower left. (F) A distant view of JW-1 boulder (arrow), showing the position of the platform sample JW-1-P (dot). (G) Imbricated boulders. Samples were collected from JW-2 boulder to the left (arrow) and an additional sample (JW-2-P) was collected from platform bedrock surface (dot). (H) Elevated, heavily jointed and unplucked bedrock platform ~500 m downstream from the upstream edge of the waterhole. Sample JW-4-BR was collected from the surface near hammer in the middle of the photo.

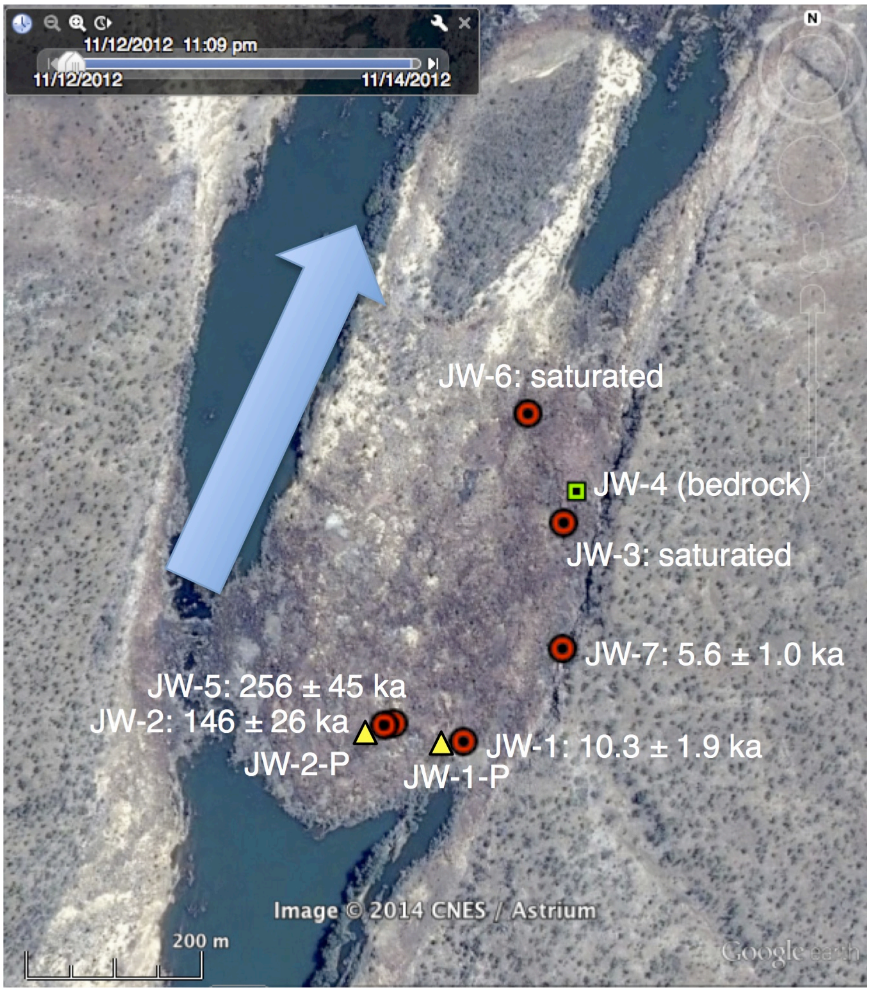


**Figure DR3.** Google image of the Jack's Waterhole with the position of the sampled boulders (red circles), bedrock (green rectangle) and platform samples (yellow triangles). Arrow indicates flow direction. The model flip ages (model C; Table 1) are shown.